International Journal of Numerical Methods for Heat & Fluid Flow

Emerald Article: Natural convection from a vertical permeable cone in a nanofluid saturated porous media for uniform heat and nanoparticles volume fraction fluxes

A.J. Chamkha, A.M. Rashad

The current issue and full text archive of this journal is available at
www.emeraldinsight.com/0961-5539.htm

Natural convection from a vertical permeable cone in a nanofluid saturated porous media for uniform heat and nanoparticles volume fraction fluxes

Received 23 March 2011
Accepted 23 May 2011

A.J. Chamkha
Manufacturing Engineering Department, The Public Authority for Applied Education and Training, Shuweikh, Kuwait, and
A.M. Rashad
Department of Mathematics, Faculty of Science, South Valley University, Aswan, Egypt

Abstract

Purpose – The purpose of this paper is to study steady, laminar, natural convection boundary-layer flow over a permeable vertical cone embedded in a porous medium saturated with a nanofluid in the presence of uniform lateral mass flux.

Design/methodology/approach – The paper studies steady, laminar, natural convection boundary-layer flow over a permeable vertical cone embedded in a porous medium saturated with a nanofluid in the presence of uniform lateral mass flux.

Findings – The presence of nanoparticles has significant effects of heat transfer.

Originality/value – The area of nanofluids is very original.

Keywords Natural convection, Porous media, Nanofluid, Cone, Thermophoresis, Brownian diffusion, Convection, Porous materials, Heat transfer

Paper type Research paper

1. Introduction

Nanofluids are prepared by dispersing solid nanoparticles in fluids such as water, oil, or ethylene glycol. These fluids represent an innovative way to increase thermal conductivity and, therefore, heat transfer. Unlike heat transfer in conventional fluids, the exceptionally high-thermal conductivity of nanofluids provides for exceptional heat transfer, a unique feature of nanofluids. Advances in device miniaturization have necessitated heat transfer systems that are small in size, light mass, and high-performance. Several authors have tried to establish convective transport models for nanofluids. A nanofluid is a two-phase mixture in which the solid phase consists of nano-sized particles. In view of the nano-scale size of the particles, it may be questionable whether the theory of conventional two-phase flow can be applied in describing the flow characteristics of nanofluid (Xuan and Roetzel, 2000). Since the size of the particles is less than 100 nm, nanofluids behave more like a fluid than a mixture (Xuan and Roetzel, 2000;

International Journal of Numerical Methods for Heat & Fluid Flow
Vol. 22 No. 8, 2012
pp. 1073-1085

0961-5539
DOI 10.1108/09615531211271871

Lee *et al.*, 1999; Maliga *et al.*, 2005). Xuan and Roetzel (2000) proposed homogeneous flow model where the convective transport equations of pure fluids are directly extended to nanofluids. This means that all traditional heat transfer correlations (e.g. Dittus-Boelter) could be used for nanofluids provided that the properties of pure fluids are replaced by those of nanofluids involving the volume fraction of the nanoparticles. The homogeneous flow models are, however, in conflict with the experimental observations of Maliga *et al.* (2005), as they under predict the heat transfer coefficient of nanofluids. Kang *et al.* (2006) studied estimation of the thermal conductivity of a nanofluid using experimental effective particle volume. Application of nanofluids for heat transfer enhancement of separated flows encountered in a backward facing step presented by Abu-Nada (2008). Numerical research of natural convective heat transfer enhancement filled with nanofluids in rectangular enclosures proposed by Jou and Tzeng (2006). Hwang *et al.* (2007) reported a buoyancy-driven heat transfer of water-based on nanofluids in a rectangular cavity. A numerical study of natural convection in partially heated rectangular enclosures filled with nanofluids was conducted by Tiwari and Das (2007). Oztop and Abu-Nada (2008) investigated a numerical study of natural convection in partially heated rectangular enclosures filled with nanofluids. The effects of inclination angle on natural convection in enclosures filled with Cu-water nanofluid studied by Abu-Nada and Oztop (2009). Duangthongsuk and Wongwises (2008) analyzed the effect of thermophysical properties models on the predicting of the convective heat transfer coefficient for low concentration nanofluid. Recently, Chamkha *et al.* (2011) studied mixed convection MHD flow of a nanofluid past a stretching permeable surface in the presence of magnetic field, heat generation or absorption, thermopherosis, Brownian motion and suction or injection effects. Chamkha *et al.* (2010) also analyzed natural convection past a sphere embedded in a porous medium saturated by a nanofluid. Gorla *et al.* (2011b) studied steady boundary layer flow of a nanofluid on a stretching circular cylinder in a stagnant free stream. Gorla *et al.* (2011a) analyzed mixed convection past a vertical wedge embedded in a porous medium saturated by a nanofluid.

The objective of the present study is to analyze the effect of uniform lateral mass flux on natural convection boundary-layer flow of a nanofluid over a permeable vertical cone embedded in a porous medium. The surface of the cone is maintained at uniform heat and nanoparticles volume fraction fluxes. The effects of nanoparticles Brownian motion and thermophoresis are included in the model.

2. Governing equations

Consider the problem of natural convection boundary-layer flow over a permeable vertical cone embedded in a porous medium saturated with a nanofluid. The model used for the nanofluid incorporates the effects of Brownian motion and thermophoresis. The cone surface is maintained at a uniform heat flux q_w and a uniform nanoparticles volume fraction flux m_w and the ambient temperature and nanoparticles volume fraction far away from the surface of the cone T_∞ and C_∞ are assumed to be uniform. Figure 1 shows the flow model and physical coordinate system. The origin of the coordinate system is placed at the vertex of the cone, where x and y are Cartesian coordinates measuring the distances along and normal to the surface of the cone, respectively. All of the fluid properties are assumed to be constant, except for density variations in the buoyancy term. By introducing the boundary layer and the Boussinesq approximations, the governing equations based on the Darcy law can be written as follows (Yih, 1997):

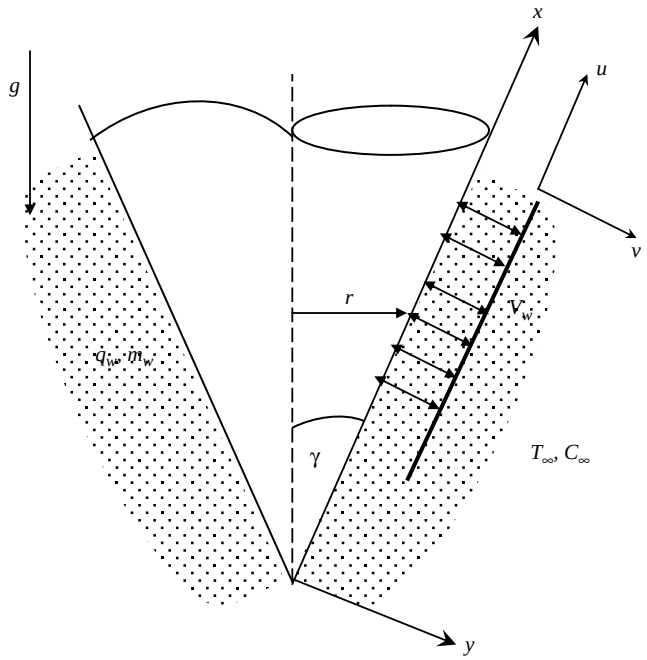

Figure 1.
Flow model and physical coordinate system

$$\frac{\partial(ru)}{\partial x}+\frac{\partial(rv)}{\partial y}=0, \tag{1}$$

$$\frac{\partial u}{\partial y}=\frac{(1-C_\infty)\rho_{f\infty}\cos\gamma\beta gK}{\mu}\cdot\frac{\partial T}{\partial y}-\frac{(\rho_p-\rho_{f\infty})\cos\gamma gK}{\mu}\cdot\frac{\partial C}{\partial y}, \tag{2}$$

$$u\frac{\partial T}{\partial x}+v\frac{\partial T}{\partial y}=\alpha\frac{\partial^2 T}{\partial y^2}+\tau\left[D_B\frac{\partial C}{\partial y}\frac{\partial T}{\partial y}+\left(\frac{D_T}{T_\infty}\right)\left(\frac{\partial T}{\partial y}\right)^2\right], \tag{3}$$

$$u\frac{\partial C}{\partial x}+v\frac{\partial C}{\partial y}=D_B\frac{\partial^2 C}{\partial y^2}+\left(\frac{D_T}{T_\infty}\right)\frac{\partial^2 T}{\partial y^2}, \tag{4}$$

where u, v, T and C are the x- and y-components of velocity, temperature and nanoparticles volume fraction, respectively. K, β, g, D_B and D_T are the permeability of the porous medium, volumetric expansion coefficient of the fluid, gravitational acceleration, Brownian diffusion coefficient and thermophoretic diffusion coefficient, respectively. γ, μ, ρ_f and ρ_p are the cone half angle, fluid viscosity, fluid density and nanoparticles mass density, respectively. $\alpha = k_m/(\rho c)_f$ and $\tau = (\rho c)_p/(\rho c)_f$ are the effective thermal diffusivity of porous medium and the ratio of heat capacities, respectively. k_m, $(\rho c)_f$ and $(\rho c)_p$ are effective thermal conductivity, heat capacity of the fluid and the effective heat capacity of nanoparticles material, respectively.

The boundary conditions suggested by the physics of the problem are given by:

$$y = 0 : v = V_w, \quad -k_m\left(\frac{\partial T}{\partial y}\right) = q_w, \quad -D_B\left(\frac{\partial C}{\partial y}\right) = m_w, \tag{5a}$$

$$y \to \infty : u = 0, \quad T = T_\infty, \quad C = C_\infty, \tag{5b}$$

where V_w is the uniform transpiration velocity. We assume that the boundary layer is sufficiently thin in comparison with the local radius of the cone. The local radius to a point in the boundary layer, therefore, can be replaced by the radius of the cone r, i.e. $r = x \sin \gamma$.

Introducing the stream function such that: $ru = \partial\psi/\partial y$, $rv = -\partial\psi/\partial x$ and invoking the following dimensionless variables:

$$\xi = \frac{2V_w x}{\alpha Ra_x^{1/3}}, \quad \eta = \frac{y}{x} Ra_x^{1/3}, \quad f(\xi, \eta) = \frac{\psi}{\alpha r Ra_x^{1/3}},$$
$$\theta(\xi, \eta) = \frac{(T - T_\infty)k_m Ra_x^{1/3}}{q_w x}, \quad \phi(\xi, \eta) = \frac{(C - C_\infty)D_B Ra_x^{1/3}}{m_w x}, \tag{6}$$

into equations (1) through (5) produce the following non-similar equations and boundary conditions:

$$f'' = \theta' - N_r\phi', \tag{7}$$

$$\theta'' + N_b\phi'\theta' + \frac{5}{3} f\theta' - \frac{1}{3} f'\theta + N_t\theta'^2 = \frac{1}{3}\xi\left(f'\frac{\partial\theta}{\partial\xi} - \theta'\frac{\partial f}{\partial\xi}\right), \tag{8}$$

$$\phi'' + \frac{5Le}{3} f\phi' - \frac{Le}{3} f'\phi + \frac{N_t}{N_b}\theta'' = \frac{Le}{3}\xi\left(f'\frac{\partial\phi}{\partial\xi} - \phi'\frac{\partial f}{\partial\xi}\right), \tag{9}$$

$$\eta = 0 : f = -\frac{\xi}{4}, \quad \theta' = -1, \quad \phi' = -1, \tag{10a}$$

$$\eta \to \infty : \theta = 0, \quad \phi = 0, \tag{10b}$$

where:

$$N_r = \frac{(\rho_p - \rho_{f\infty})m_w k_m Ra_x^{1/3}}{(1 - C_\infty)\rho_{f\infty}\beta q_w D_B}, \quad N_b = \frac{(\rho c)_p m_w x}{(\rho c)_f \alpha Ra_x^{1/3}}, \quad N_t = \frac{(\rho c)_p D_T q_w x}{(\rho c)_f \alpha T_\infty k_m Ra_x^{1/3}},$$
$$Le = \frac{\alpha}{D_B}, \quad Ra_x = \left(\frac{(1 - C_\infty)\rho_{f\infty} g \cos\gamma\beta K q_w x^2}{\mu k_m \alpha}\right) \tag{11}$$

are the buoyancy ratio, Brownian motion parameter, thermophoresis parameter, Lewis number, and the modified local Rayleigh number, respectively. It should be noted that the wall mass flux parameter $\xi = 0$ ($V_w = 0$) corresponds to impermeable cone surface while $\xi > 0$ ($V_w > 0$) corresponds to the case of fluid injection (present work) and $\xi < 0$ ($V_w < 0$) corresponds to the case of fluid suction.

Of special significance for this problem are the local Nusselt and Sherwood numbers. These physical quantities can be defined as:

$$Nu_x Ra_x^{-1/3} = \frac{1}{\theta(\xi, 0)}, \tag{12}$$

$$Sh_x Ra_x^{-1/3} = \frac{1}{\phi(\xi, 0)}. \tag{13}$$

3. Numerical method and validation

Equations (7) through (9) represent an initial-value problem with ξ playing the role of time. This general non-linear problem cannot be solved in closed form and, therefore, a numerical solution is necessary to describe the physics of the problem. The implicit, tri-diagonal finite-difference method similar to that discussed by Blottner (1970) has proven to be adequate and sufficiently accurate for the solution of this kind of problems. Therefore, it is adopted in the present work. All first-order derivatives with respect to ξ are replaced by two-point backward-difference formulae when marching in the positive ξ direction. Then, all second-order differential equations in η are discretized using three-point central difference quotients. This discretization process produces a tri-diagonal set of algebraic equations at each line of constant ξ which is readily solved by the well known Thomas algorithm (Blottner, 1970). During the solution, iteration is employed to deal with the non-linearity aspect of the governing differential equations. The problem is solved line by line starting with line $\xi = 0$ where similarity equations are solved to obtain the initial profiles of velocity, temperature and nanoparticles volume fraction and marching forward in ξ until the desired line of constant ξ is reached. Variable step sizes in the η direction with $\Delta\eta_1 = 0.001$ and a growth factor $G = 1.035$ such that $\Delta\eta_n = G\Delta\eta_{n-1}$ and constant step sizes in the ξ direction with $\Delta\xi = 0.01$ are employed. These step sizes are arrived at after many numerical experimentations performed to assess grid independence. The convergence criterion employed in the present work is based on the difference between the current and the previous iterations. When this difference reached 10^{-5} for all points in the η directions, the solution was assumed converged and the iteration process was terminated. The above step sizes and convergence criterion were found to give accurate grid-independent results as verified by the comparison mentioned below.

In order to access the accuracy of the numerical results, we have compared the results obtained by this numerical method with the previously published work of Yih (1997) for various values of ξ in the absence of nanoparticles volume fraction flux (i.e. $N_r = N_b = N_t = 0$). This comparison is presented in Table I. It is obvious from this table that excellent agreement between the results exists. This favourable comparison lends confidence in the graphical results to be reported in the next section.

Table I. Values of $\theta(\xi, 0)$ for various values of ξ in the absence of nanoparticles volume fraction flux (i.e. $N_r = N_b = N_t = 0$)

ξ	Yih (1997)	Present results
0	0.7686	0.76865
2	0.3537	0.35374
4	0.1342	0.13425
6	0.0400	0.04006
8	0.0092	0.00923
10	0.0016	0.00164

4. Results and discussion

In this section, a representative set of graphical results for the dimensionless velocity $f'(\xi, \eta)$, temperature $\theta(\xi, \eta)$, and nanoparticles volume fraction $\phi(\xi, \eta)$ as well as the local Nusselt number $Nu_x Ra_x^{-1/3} = 1/\theta(\xi, 0)$ (reciprocal of wall temperature), and the local Sherwood number $Sh_x Ra_x^{-1/3} = 1/\phi(\xi, 0)$ (reciprocal of wall nanoparticles volume fraction) is shown in Figures 2 through 13 and discussed for various parametric conditions. These conditions are intended for various values of the buoyancy ratio N_r, Brownian motion parameter N_b, thermophoresis parameter N_t, Lewis number Le and the wall mass flux parameter ξ.

Figure 2(a)-(c) shows the effects of the buoyancy ratio N_r on the velocity f', temperature θ and nanoparticles volume fraction ϕ, respectively. It can be seen that increases in the value of the buoyancy ratio N_r has a tendency to decelerate the fluid flow along the cone surface. This is reflected in the decreases in the fluid velocity in the immediate vicinity of the cone surface as N_r increases. This behavior in the flow velocity is accompanied by slight increases in the fluid temperature and nanoparticles volume fraction as N_r increases from 0.1 to 0.7. On the other hand, Figures 3 and 4 show the influence of the buoyancy ratio N_r on the local Nusselt number $Nu_x Ra_x^{-1/3}$ and the local Sherwood number $Sh_x Ra_x^{-1/3}$, for various values of the wall mass flux parameter ξ, respectively. The increases in the fluid temperature and volume fraction profiles as N_r increases mentioned above causes the values of the wall temperature and wall nanoparticles volume fraction to increase yielding decreases in both the local Nusselt and Sherwood numbers. In addition, it is observed that both of the local Nusselt and Sherwood numbers decrease with increasing values of ξ.

Figure 5(a)-(c) display the effects of increasing the Brownian motion parameter N_b on the velocity, temperature and nanoparticles volume fraction profiles, respectively. It can be observed that increasing the value of the Brownian motion parameter N_b causes increases in both of the velocity and temperature profiles especially in the

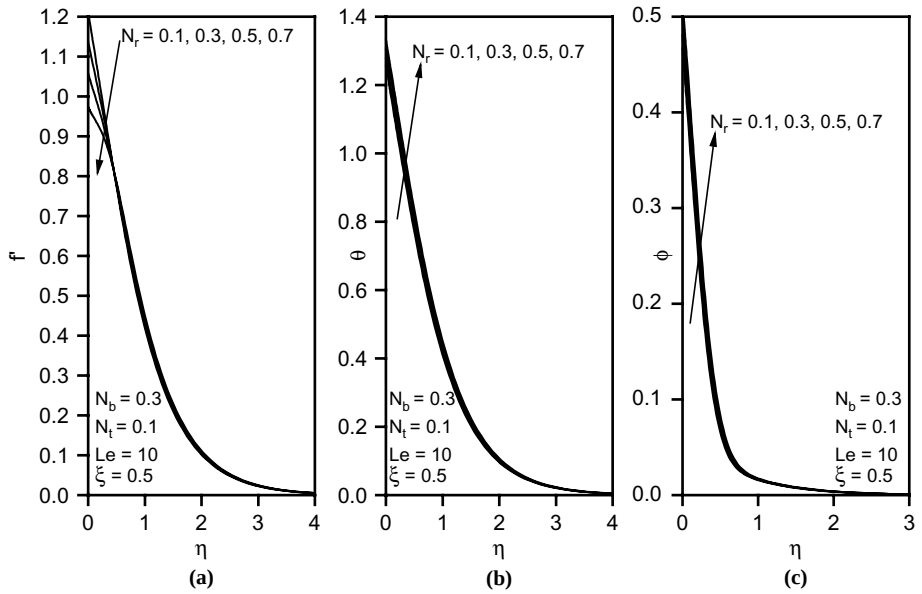

Figure 2.
Effect of N_r on the (a) velocity, (b) temperature, (c) volume fraction profiles

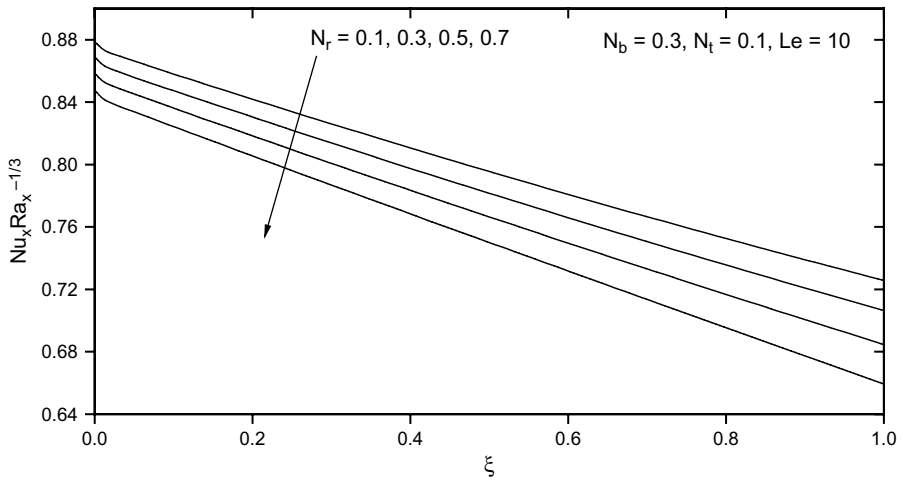

Figure 3.
Effect of N_r on the local Nusselt number

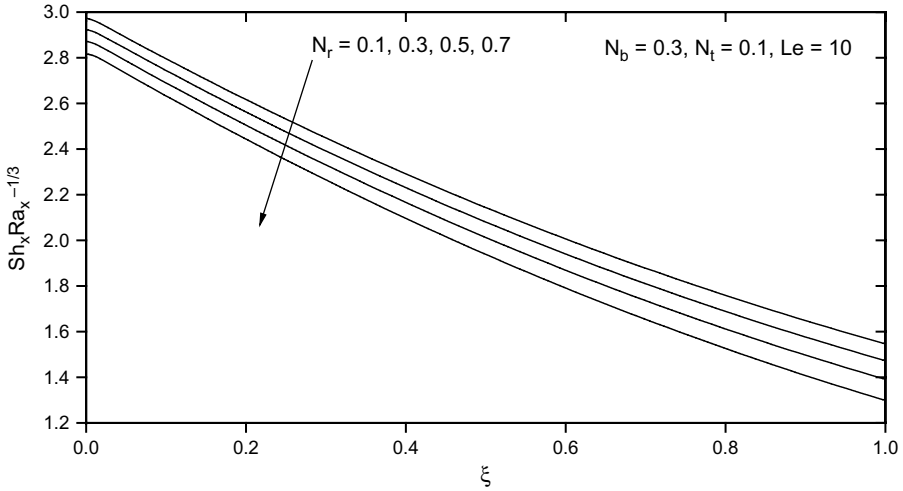

Figure 4.
Effect of N_r on the local Sherwood number

region close to the cone surface with a significant decrease in the nanoparticles volume fraction profiles. These behaviors are clearly shown in Figure 5(a)-(c).

Figures 6 and 7 show the effects of the Brownian motion parameter N_b on the local Nusselt number $Nu_x Ra_x^{-1/3}$ and local Sherwood number $Sh_x Ra_x^{-1/3}$ for different values of the wall mass flux parameter ξ, respectively. As indicated before, increasing the Brownian motion parameter N_b causes the fluid temperature to increase while the nanoparticles volume fraction decreases. This yields a consequent reduction in the local Nusselt number and an enhancement in the local Sherwood number as they are inversely proportional to the wall temperature and nanoparticles volume fraction (equations (12) and (13)), respectively.

Figure 8(a)-(c) present the velocity, temperature and nanoparticles volume fraction profiles for various values of the thermophoresis parameter N_t, respectively. Increases in

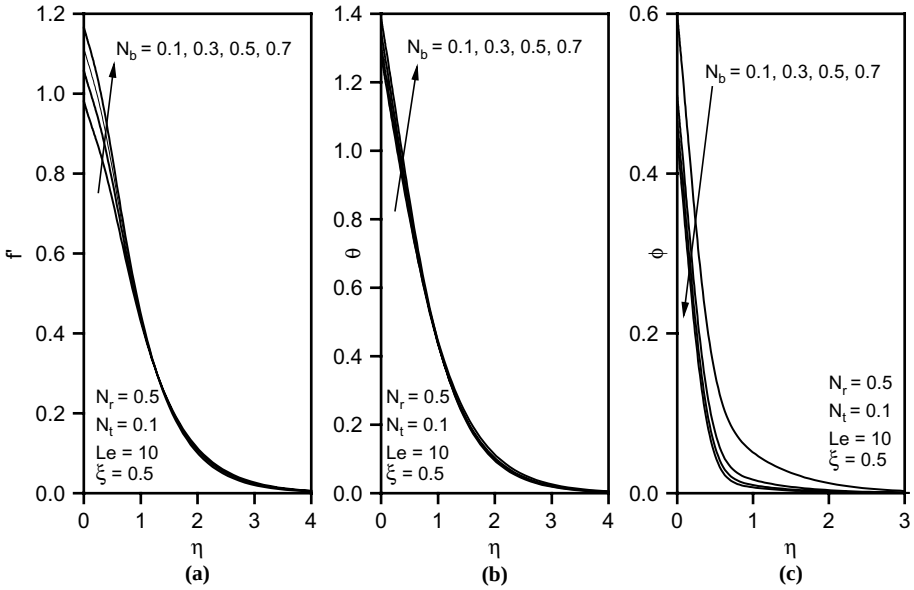

Figure 5.
Effect of N_b on the (a) velocity, (b) temperature, (c) volume fraction profiles

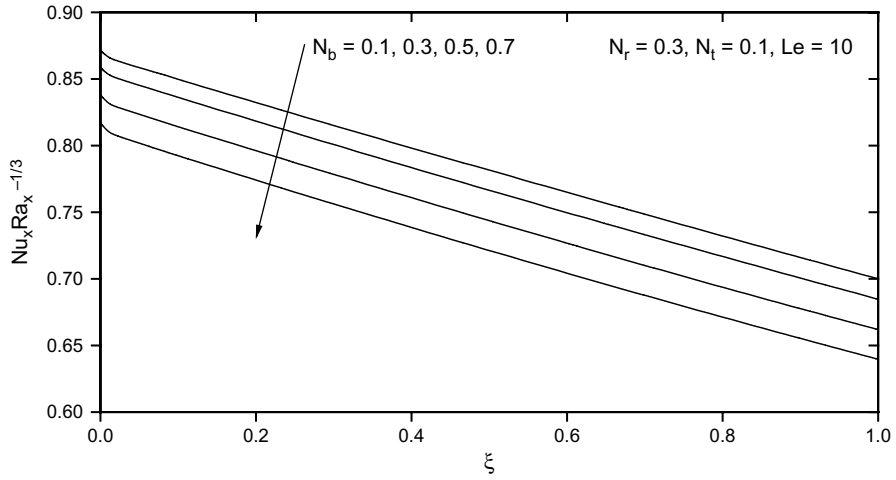

Figure 6.
Effect of N_b on the local Nusselt number

the thermophoresis parameter N_t have the tendency to increase the velocity profiles as well as the fluid temperature and nanoparticles volume fraction profiles. As observed from Figure 8(a)-(c), the effect of the thermophoresis parameter N_t is more pronounced of the nanoparticles volume fraction profiles than on the fluid velocity and temperature.

Figures 9 and 10 show the effect of the thermophoresis parameter N_t on the values of local Nusselt and Sherwood numbers $Nu_x Ra_x^{-1/3}$ and $Sh_x Ra_x^{-1/3}$ for various values of the wall mass flux parameter ξ, respectively. As mentioned before, in general for small values of ξ, increasing the value of the thermophoresis parameter N_t results in

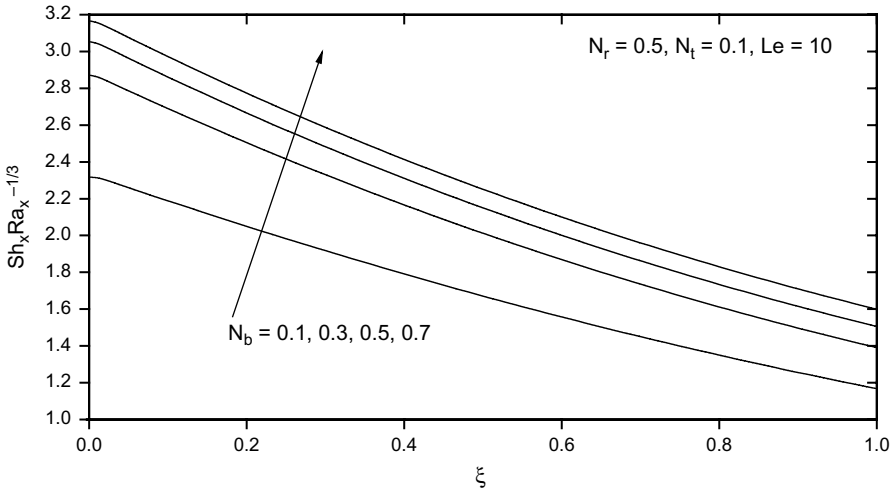

Figure 7.
Effect of N_b on the local Sherwood number

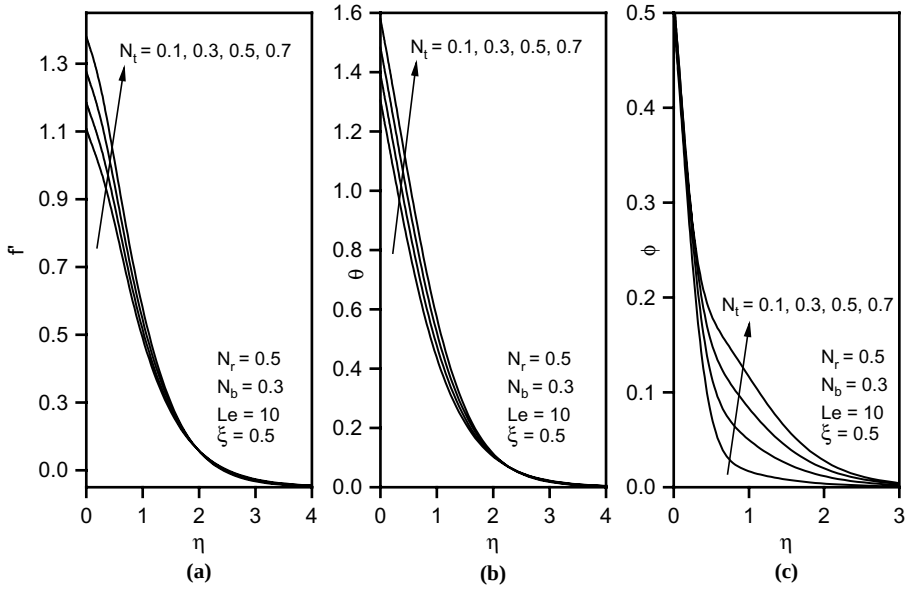

Figure 8.
Effect of N_t on the (a) velocity, (b) temperature, (c) volume fraction profiles

increasing both the wall temperature and nanoparticles volume fraction causing the values of both $Nu_xRa_x^{-1/3}$ and $Sh_xRa_x^{-1/3}$ to decrease, respectively, as N_t increases. However, while this behavior in the local Nusselt number is true for all considered values of ξ, it is not so for the behavior of the local Sherwood number. It is predicted that as both of N_t and ξ increase the behavior of the local Sherwood number changes. For example, for values of ξ in the range $0 \leq \xi \leq 0.45$, the local Shewood number decreases as N_t increases from 0.3 to 0.5 while it increases as ξ is increased further. Thus, it is concluded that the values of $Sh_xRa_x^{-1/3}$ decrease for no or weak fluid wall

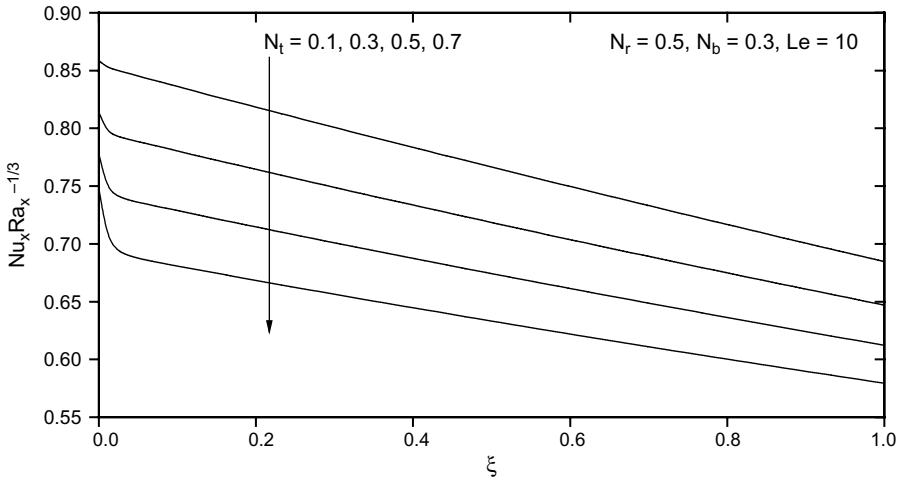

Figure 9.
Effect of N_t on the local Nusselt number

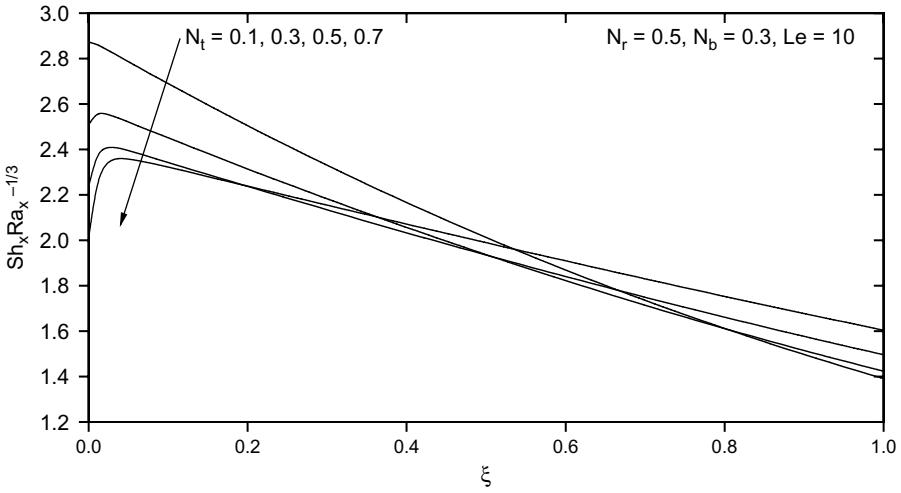

Figure 10.
Effect of N_t on the local Sherwood number

injection $0 \leq \xi \leq 0.17$ while they increase for strong fluid wall injection $0.8 \leq \xi \leq 1.0$ as N_t is increased from 0.1 to 0.7. These behaviors are clearly shown in Figure 10.

Figure 11(a)-(c) show representative fluid velocity, temperature and nanoparticles volume fraction profiles for different values of the Lewis number *Le*, respectively. It is clearly noted that the velocity increases while both the fluid temperature and nanoparticles volume fraction as well as its boundary-layer thickness decrease considerably as the Lewis number *Le* increases.

Finally, Figures 12 and 13 present the effects of the Lewis number *Le* on the local Nusselt number $Nu_xRa_x^{-1/3}$ and the local Sherwood number $Sh_xRa_x^{-1/3}$, for different values of the wall mass flux parameter ξ, respectively. As mentioned before, increasing the Lewis number *Le* causes reductions in the wall fluid temperature and the nanoparticles

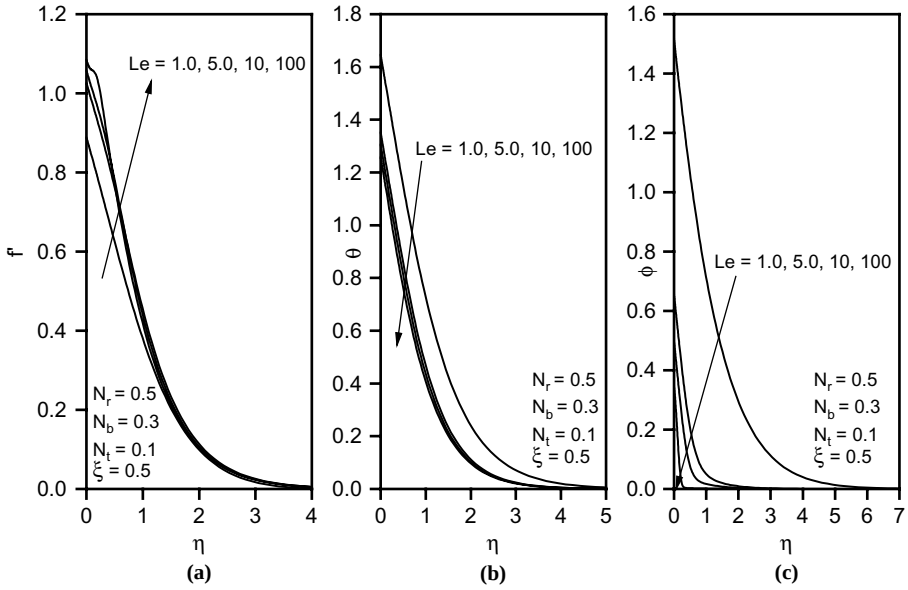

Figure 11.
Effect of Le on the (a) velocity, (b) temperature, (c) volume fraction profiles

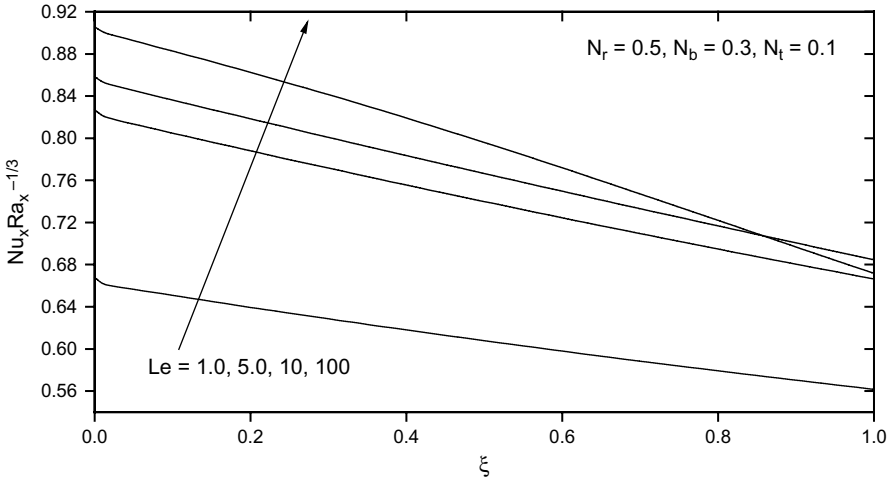

Figure 12.
Effect of Le on the local Nusselt number

volume fraction which yield a consequent enhancements in both the heat and mass transfer effects represented by increases in the local Nusselt and Sherwood numbers.

5. Conclusion

In the present work, we studied theoretically the problem of steady natural convection flow of a nanofluid over a permeable vertical cone subjected to uniform heat and nanoparticles volume fraction fluxes and embedded in a porous medium in the presence of uniform lateral mass flux effect. The model used for the nanofluid

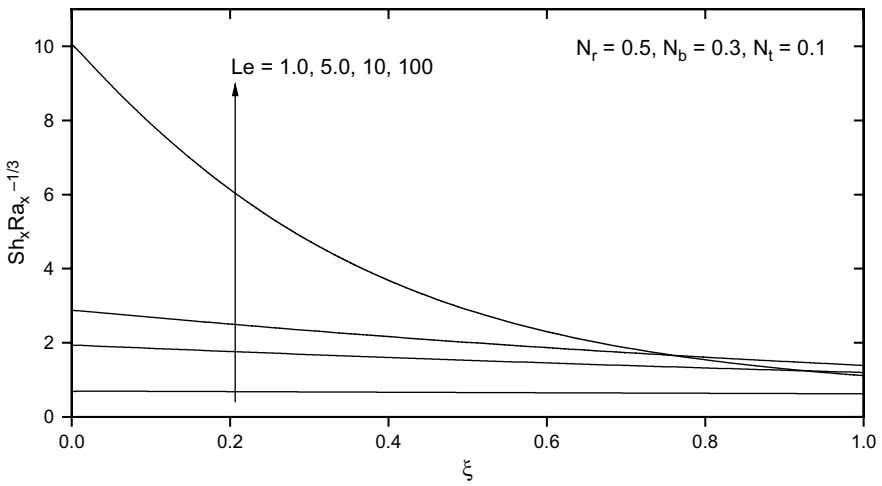

Figure 13.
Effect of Le on the local Sherwood number

incorporates the effects of Brownian motion and thermophoresis. The obtained non-similar differential equations were solved numerically by an efficient implicit finite-difference method. A comparison with previously published work was done and the results were found to be in excellent agreement. The results focused on the effects of the buoyancy ratio, Brownian motion parameter, thermophoresis parameter and Lewis number for different wall lateral mass flux parameters on the local Nusselt and Sherwood numbers. It was found that as either the buoyancy ratio or the wall mass flux parameter was increased, both the local Nusselt and Sherwood numbers decreased. In addition, it was concluded that as the Brownian motion parameter increased, the local Nusselt number decreased while the local Sherwood number increased. However, they both decreased as the thermophoresis parameter increased for no or weak fluid wall injection effects while the local Sherwood number took on the opposite behavior for strong fluid wall injection effects. In addition, increasing the Lewis number produced increases in both of the local Nusselt and Sherwood numbers.

References

Abu-Nada, E. (2008), "Application of nanofluids for heat transfer enhancement of separated flows encountered in a backward facing step", *Int. J. Heat Fluid Flow*, Vol. 29, pp. 242-49.

Abu-Nada, E. and Oztop, H.F. (2009), "Effects of inclination angle on natural convection in enclosures filled with Cu-water nanofluid", *Int. J. Heat and Fluid Flow*, Vol. 30, pp. 669-78.

Blottner, F.G. (1970), "Finite-difference methods of solution of the boundary-layer equations", *AIAA Journal*, Vol. 8, pp. 193-205.

Chamkha, A.J., Aly, A.M. and Al-Mudhaf, H. (2011), "Laminar MHD mixed convection flow of a nanofluid along a stretching permeable surface in the presence of heat generation or absorption effects", *International Journal of Microscale and Nanoscale Thermal and Fluid Transport Phenomena*, Vol. 2 No. 1.

Chamkha, A.J., Gorla, R.S.R. and Ghodeswar, K. (2010), "Non-similar solution for natural convective boundary layer flow over a sphere embedded in a porous medium saturated with a nanofluid", *Transport in Porous Media*, Vol. 86, pp. 13-22.

Duangthongsuk, W. and Wongwises, S. (2008), "Effect of thermophysical properties models on the predicting of the convective heat transfer coefficient for low concentration nanofluid", *Int. Commun. Heat Mass Transfer*, Vol. 35, pp. 1320-26.

Gorla, R.S.R., Chamkha, A.J. and Rashad, A.M. (2011a), "Mixed convective boundary layer flow over a vertical wedge embedded in a porous medium saturated with a nanofluid", *Journal of Nanoscale Research Letters*, Vol. 6 No. 1.

Gorla, R.S.R., EL-Kabeir, S.M.M. and Rashad, A.M. (2011b), "Heat transfer in the boundary layer on a stretching circular cylinder in a nanofluid", *Journal of Thermophysics and Heat Transfer*, Vol. 25, pp. 183-86.

Hwang, K.S., Lee, J.-H. and Jang, S.P. (2007), "Buoyancy-driven heat transfer of water-based Al nanofluids in a rectangular cavity", *Int. J. Heat Mass Transfer*, Vol. 50, pp. 4003-10.

Jou, R.Y. and Tzeng, S.C. (2006), "Numerical research of nature convective heat transfer enhancement filled with nanofluids in rectangular enclosures", *Int. Commun. Heat Mass Transfer*, Vol. 33, pp. 727-36.

Kang, H.U., Kim, S.H. and Oh, J.M. (2006), "Estimation of thermal conductivity of nanofluid using experimental effective particle volume", *Experimental Heat Transfer*, Vol. 19, pp. 181-91.

Lee, S., Choi, S.U.S., Li, S. and Eastman, J.A. (1999), "Measuring thermal conductivity of fluids containing oxide nanoparticles", *ASME Trans. J. Heat Transfer*, Vol. 121, pp. 280-89.

Maliga, S.E.B., Palm, S.M., Nguyen, C.T., Roy, G. and Galanis, N. (2005), "Heat transfer enhancement using nanofluid in forced convection flow", *Int. J. Heat Fluid Flow*, Vol. 26, pp. 530-46.

Oztop, H.F. and Abu-Nada, E. (2008), "Numerical study of natural convection in partially heated rectangular enclosures filled with nanofluids", *Int. J. Heat Mass Transfer*, Vol. 29, pp. 1326-36.

Tiwari, R.K. and Das, M.K. (2007), "Heat transfer augmentation in a two-sided lid-driven differentially heated square cavity utilizing nanofluids", *Int. J. Heat Mass Transfer*, Vol. 50, pp. 2002-18.

Xuan, Y. and Roetzel, W. (2000), "Conceptions for heat transfer correlation of nanofluids", *Int. J. Heat Mass Transfer*, Vol. 43, pp. 3701-07.

Yih, K.A. (1997), "The effect of uniform lateral mass flux on free convection about a vertical cone embedded in a saturated porous medium", *Int. Comm. Heat Mass Transfer*, Vol. 24 No. 8, pp. 1195-205.

Corresponding author
A.J. Chamkha can be contacted at: achamkha@yahoo.com